6th European Conference on Computational Mechanics (ECCM 6)
7th European Conference on Computational Fluid Dynamics (ECFD 7)
11-15 June 2018, Glasgow, UK

HIGH-ORDER ACCURATE TIME INTEGRATION METHODS FOR ELECTROMAGNETIC-THERMAL ANALYSIS

Tobias Gleim[1] **and Detlef Kuhl**[1]

[1] Chair of Mechanics and Dynamics, University of Kassel, Mönchebergstrae 7, 34109 Kassel,
tgleim@uni-kassel.de, kuhl@uni-kassel.de

Key words: MAXWELL equations, electromagnetic induction, high-order accurate integration schemes, GALERKIN time integration methods, RUNGE-KUTTA time integration methods, residual error estimator

Abstract. The present paper aims at investigating a high-order time integration method with an appropriate error estimator in the context of an induction heating process. Therefore, an axisymmetric model problem of a metal shaft with a surrounding copper coil is investigated. In order to describe the proceeding a thermo-electromagnetic multifield problem is introduced. MAXWELL's equations are coupled and linked to the heat conduction equation due to JOULE's effect. The coupling of the nonlinear MAXWELL equations and the heat conduction equation results in a monolithic multifield problem. The resulting equations are discretized using high-order accurate finite elements in space as well as in time. Finally, the time discretization error is estimated and classified employing a residual error estimate.

1 MOTIVATION

In order to achieve application-optimized material properties, new material composites or novel fabrication sequences are developed. Thus, in the area of metal-forming processes, heating and cooling strategies that locally influence workpiece characteristics such as ductility, hardness, yield strength or impact resistance, are important concepts. Hence, a special profile of characteristics can be adapted to the intended load profile of the component. For example, high strength can be achieved at a predetermined position, while particularly good wear or damping properties predominate in other places. The tailor-made combination of properties has been realized in the past by a variety of different materials or extensive manufacturing processes. For components made with just one metal, precisely defined properties can be obtained in the following three stages, see **Figure 1**. In this integrated manufacturing process, a metal shaft obtains a heterogenous temperature distribution throughout a local inductive heating. Then the heated metal shaft is formed in a press and simultaneously cooled due to the contact with the die. Finally, the desired material properties are achieved by partial rapid cooling, allowing the creation of graded materials with defined properties, cf. [20]. Investigations and studies

Figure 1: Integrated thermomechanical forming process, cf. [20]

with respect to high-order time integration methods for this process chain can be found in [9, 10, 18, 3].

The first step of this fabrication sequence will be analyzed, acknowledging that a material gradation is only enabled due to the inhomogeneous temperature distribution obtained by inductive heating. The prediction of this process step will be realized by solving Maxwell's equations as well as the heat conduction equation using Galerkin's method with high-order accurate approaches in space and time in conjunction with an adequate error estimator.

Nevertheless, in literature a bunch of other solution strategies are available. Within the analysis of electromagnetic phenomena they emerge from different formulations of Maxwell's equations and contain extraordinary element approaches, cf. [1, 6]. A popular time integration scheme for solving the semidiscrete balance equation for electromagnetic problems is the time integration method of Crank Nicholson, cf. [1, 4, 11]. Similarly, the classical implicit Euler method, cf. [11], or other finite-difference-based approaches, cf. [7], are used to solve the problem.

On the contrary in the area of linear heat conduction discontinuous and continuous Galerkin methods can be found for time integration, cf. [14]. Since an analytical solution of this coupled thermo-electro multfield problem can not be obtained easily, appropriate tactics for estimating the various prevailing discretization errors have to be established. Existing approaches consider Taylor series expansions, energy evaluations, dual problem formulations, residual error determination and error definitions exploiting both the h- as well as p-version of Galerkin's method, cf. [13, 19, 2, 8, 15]. Moreover, the residual error estimator, which was originally proposed by [2], will be adapted and analyzed within the context of the inductive heating problem.

2 The Thermo-Electromagnetic Equations

Electromagnetic phenomena are generally depicted by Maxwell's equations. They are a set of partial differential equations in space and time. These equations deal with electric and magnetic aspects, including their interaction. Since the electric and magnetic fields vary in time, reciprocal actions are induced. The following four time- and space-

dependent vector fields are introduced:

$$\nabla \cdot \boldsymbol{D}(\boldsymbol{X},t) = \rho_{\mathrm{R}}(\boldsymbol{X},t) \qquad \forall \boldsymbol{X} \in \Omega_E, \quad \forall t \in [t_0,T], \tag{1}$$

$$\nabla \cdot \boldsymbol{B}(\boldsymbol{X},t) = 0 \qquad \forall \boldsymbol{X} \in \Omega_B, \quad \forall t \in [t_0,T], \tag{2}$$

$$\nabla \times \boldsymbol{H}(\boldsymbol{X},t) = \boldsymbol{J}(\Theta,\boldsymbol{X},t) + \dot{\boldsymbol{D}}(\boldsymbol{X},t) \qquad \forall \boldsymbol{X} \in \Omega_{E,B}, \quad \forall t \in [t_0,T], \tag{3}$$

$$\nabla \times \boldsymbol{E}(\boldsymbol{X},t) = -\dot{\boldsymbol{B}}(\boldsymbol{X},t) \qquad \forall \boldsymbol{X} \in \Omega_{E,B}, \quad \forall t \in [t_0,T], \tag{4}$$

The variable $\boldsymbol{E}$ represents the electric field intensity, $\boldsymbol{D}$ the electric flux density, $\boldsymbol{H}$ the magnetic field intensity, $\boldsymbol{B}$ the magnetic flux density, ρ_R the electric charge density in a volume and $\boldsymbol{J}$ the electric current density in a surface. Those variables can be dependent on the temperature Θ, the spatial position $\boldsymbol{X}$ and the time t. Some of the variables included in the MAXWELL equations are not independent of each other; they are connected, assuming the following constitutive laws, [5].

$$\boldsymbol{D}(\boldsymbol{X},t) = \epsilon\, \boldsymbol{E}(\boldsymbol{X},t) \qquad \forall \boldsymbol{X} \in \Omega_E, \quad \forall t \in [t_0,T] \tag{5}$$

$$\boldsymbol{B}(\boldsymbol{X},t) = \mu(\Theta)\boldsymbol{H}(\boldsymbol{X},t) \qquad \forall \boldsymbol{X} \in \Omega_B, \quad \forall t \in [t_0,T] \tag{6}$$

$$\boldsymbol{J}(\Theta,\boldsymbol{X},t) = \sigma(\Theta)\boldsymbol{E}(\boldsymbol{X},t) + \boldsymbol{J}_{\mathrm{i}}(\boldsymbol{X},t) \qquad \forall \boldsymbol{X} \in \Omega_E, \quad \forall t \in [t_0,T] \tag{7}$$

Here, $\epsilon = \epsilon_0\epsilon_{\mathrm{R}}$ represents the permittivity, consisting of the constant electric permittivity in a vacuum ϵ_0 and a material-dependent part ϵ_{R}. The magnetic permeability $\mu = \mu_0\mu_{\mathrm{R}}$ can also be determined with the help of the constant vacuum-specific value μ_0 and a material dependent part μ_{R}. The quantity σ describes the electric conductivity.

The temperature development of the inductive heating process can be described by the heat conduction equation

$$\rho\, c_{\mathrm{p}}(\Theta)\, \dot{\Theta}(\boldsymbol{X},t) + \nabla \cdot \boldsymbol{q}(\Theta,\boldsymbol{X},t) = Q(\Theta,\boldsymbol{X},t) \qquad \forall \boldsymbol{X} \in \Omega_\Theta, \quad \forall t \in [t_0,T]. \tag{8}$$

Further introduced variables are the density ρ, the heat capacity c_{p}, the heat flux vector $\boldsymbol{q}(\Theta,\boldsymbol{X},t) = -\lambda(\Theta)\, \nabla\Theta(\boldsymbol{X},t)$, the heat source term Q and the thermal conductivity λ.

In general, in an inductive heating process a metal workpiece is surrounded by an induction coil, on which an alternating current is applied, cf. [17]. Due to the alternating current density, the magnetic vortex field is generated, which induces eddy currents. These, in turn, produce a temperature increase in the workpiece. This phenomenon is called JOULE heating and can be described by the heat equation (8) with the heat source term

$$Q(\Theta,\boldsymbol{X},t) = \frac{\boldsymbol{J}^2(\Theta,\boldsymbol{X},t)}{\sigma(\Theta)}. \tag{9}$$

As seen above, the coupling between the electric and the thermal field is clearly visible by means of the heat source term. On the other hand, the electromagnetic field is not directly coupled to the thermal field. The thermal influence on the electromagnetic field is caused by the temperature dependence of the material parameters within the constitutive laws (5) - (7). The material dependent material models, which are used for studies in the present paper, can be found in [9].

3 NUMERICAL REALIZATION

3.1 WEAK FORMULATION OF INDUCTIVE HEATING

In order to enable the application of the finite element method, the previously elaborated partial differential equations (1) - (9) as well as the NEUMANN boundary conditions have to be formulated weakly throughout a multiplication with arbitrary test functions $\delta\mathbf{E}$, $\delta\mathbf{B}$ or $\delta\Theta$ and an integration over the volume Ω. Furthermore, the strategy of DEMKOWICZ and ASSOUS, cf. [6, 1] is applied in the thermo-electromagnetic case with nonlinear material parameters, [9]. This lead to the following weak form of the electric, magnetic and thermal fields:

$$\begin{aligned}
\delta W^{\mathrm{E}} = &\int_{\Omega} \delta\boldsymbol{E}\cdot\epsilon\,\ddot{\boldsymbol{E}}\;d\mathrm{V} + \int_{\Omega}\delta\boldsymbol{E}\cdot\sigma(\Theta)\,\dot{\boldsymbol{E}}\;d\mathrm{V} + \int_{\Omega}\delta\boldsymbol{E}\cdot\dot{\sigma}(\Theta)\,\boldsymbol{E}\;d\mathrm{V} - \int_{\Omega}\nabla\cdot\delta\boldsymbol{E}\;\frac{\kappa\,\rho_{\mathrm{R}}}{\epsilon}\;d\mathrm{V}\\
&+\int_{\Omega}\kappa(\Theta)\,[\nabla\times\delta\boldsymbol{E}]\cdot[\nabla\times\boldsymbol{E}]\;d\mathrm{V} + \int_{\Omega}[\nabla\kappa(\Theta)\times\delta\boldsymbol{E}]\cdot[\nabla\times\boldsymbol{E}]\;d\mathrm{V}\\
&+\int_{\Omega}\delta\boldsymbol{E}\cdot\dot{\kappa}(\Theta)\,[\nabla\times\boldsymbol{B}]\;d\mathrm{V} + \int_{\Omega}\delta\boldsymbol{E}\cdot[\nabla\dot{\kappa}(\Theta)\times\boldsymbol{B}]\;d\mathrm{V} + \int_{\Omega}\delta\boldsymbol{E}\cdot\dot{\boldsymbol{J}}_{\mathrm{i}}\;d\mathrm{V} \qquad (10)\\
&+\int_{\Omega}\nabla\cdot\delta\boldsymbol{E}\;\kappa(\Theta)\;\nabla\cdot\boldsymbol{E}\;d\mathrm{V} + \int_{\Gamma_{\sigma\mathrm{E}}}\delta\boldsymbol{E}\cdot[\boldsymbol{n}\times[\nabla\times\boldsymbol{E}]]\;d\mathrm{A} = 0,\\
\delta W^{\mathrm{B}} = &\int_{\Omega}\delta\boldsymbol{B}\cdot\epsilon\,\ddot{\boldsymbol{B}}\;d\mathrm{V} + \int_{\Omega}[\nabla\times\delta\boldsymbol{B}]\cdot\kappa(\Theta)\,[\nabla\times\boldsymbol{B}]\;d\mathrm{V} - \int_{\Omega}\delta\boldsymbol{B}\cdot\nabla\times\sigma(\Theta)\boldsymbol{E}\;d\mathrm{V}\\
&+\int_{\Omega}[\nabla\times\delta\boldsymbol{B}]\cdot[\nabla\kappa(\Theta)\times\boldsymbol{B}]\;d\mathrm{V} + \int_{\Omega}\nabla\cdot\delta\boldsymbol{B}\;\kappa(\Theta)\;\nabla\cdot\boldsymbol{B}\;d\mathrm{V} \qquad (11)\\
&-\int_{\Omega}[\nabla\times\delta\boldsymbol{B}]\;\cdot\boldsymbol{J}_{\mathrm{i}}\;d\mathrm{V} + \int_{\Gamma_{\sigma\mathrm{B}}}\delta\boldsymbol{B}\cdot[\boldsymbol{n}\times[\nabla\times\boldsymbol{B}]]\;d\mathrm{A} = 0,\\
\delta W^{\Theta} = &\int_{\Omega}\delta\Theta\;\rho\;c_{\mathrm{p}}(\Theta)\;\dot{\Theta}\;d\mathrm{V} - \int_{\Omega}\nabla\delta\Theta\cdot\boldsymbol{q}(\Theta)\;d\mathrm{V} - \int_{\Omega}\delta\Theta\;Q\;d\mathrm{V} \qquad (12)\\
&+\int_{\Gamma_{\mathrm{q}}}\delta\Theta\left[q^{\star} + \alpha(\Theta)\,[\Theta-\Theta_{\infty}] + \varepsilon(\Theta)\;\sigma_{\Theta}\;A\;\left[\Theta^4-\Theta_{\infty}^4\right]\right]d\mathrm{A} = 0.
\end{aligned}$$

The dependencies of the variables with respect to the spatial position and time are omitted for simplicity.

Since high temperatures occur in the inductive heating process and heat exchange with the environment occurs, equation (12) considers free convection and thermal radiation. The heat transfer coefficient $\alpha(\Theta)$ as well as the emissivity $\varepsilon(\Theta)$ have temperature dependent behaviors. The material dependent material models, which are used for studies in this paper, can be found in [9]. Furthermore, the STEFAN-BOLTZMANN constant σ_{Θ} is introduced.

Adding equations (10) - (12) results in the weakly formulated nonlinear problem

$$\delta W(\ddot{\boldsymbol{u}},\dot{\boldsymbol{u}},\boldsymbol{u}) = 0, \qquad \text{with } \boldsymbol{u} = [\boldsymbol{E},\boldsymbol{B},\Theta]^T. \qquad (13)$$

Therein the vector $\boldsymbol{u} = [\boldsymbol{E}, \boldsymbol{B}, \Theta]^T$ of primary variables is introduced together with its time derivatives to obtain this abridged form, which will also be advantageous for the compact formulation of spatial and temporal integration schemes later on. A Newton-Raphson method is considered for this nonlinear problem (13). Consequently, the consistent linearization of the virtual work δW (13) is realized by developing a TAYLOR series expansion up to the linear term, which means that higher order terms are omitted. Thus, the weak form is linearized, exploiting the GÂTEAUX derivative, cf. [12].

To complete the initial value problem for the induction heating, adequate initial conditions at the beginning of the observation at time t_0 in the domain Ω have to be complied.

$$\ddot{\boldsymbol{u}}(\boldsymbol{X}, t_0) = \ddot{\boldsymbol{u}}_0, \qquad \dot{\boldsymbol{u}}(\boldsymbol{X}, t_0) = \dot{\boldsymbol{u}}_0, \qquad \boldsymbol{u}(\boldsymbol{X}, t_0) = \boldsymbol{u}_0 \tag{14}$$

3.2 SPATIAL DISCRETIZATION

In order to solve the thermal-electromagnetic problem numerically the next step is to discretize the weak form spatially by using the finite element method. Due to the spatial discretization the whole domain Ω is divided into several finite elements e. The distinct continuous field variables are thus described with the help of discrete nodal values and vector-valued shape functions $\boldsymbol{N}_l^i = N^i \boldsymbol{e}_l$. They consist of LAGRANGE shape functions N^{i} of polynomial degree p with $i \in [1, NN]$, cf. [21], and accompanying basis vectors $\boldsymbol{e}_l$, which enable the approximation of different spatial directions $l \in [1, ND]$. In the case of three different spatial directions standard cartesian bases vectors $\boldsymbol{e}_1 = [1,0,0]^T$, $\boldsymbol{e}_2 = [0,1,0]^T$ and $\boldsymbol{e}_3 = [0,0,1]^T$ are considered.

$$\ddot{\boldsymbol{E}}(\boldsymbol{\xi}) \approx \sum_{i=1}^{NN} \sum_{l=1}^{ND} \ddot{E}_l^{\mathrm{e}i} \boldsymbol{N}_l^i(\boldsymbol{\xi}), \quad \dot{\boldsymbol{E}}(\boldsymbol{\xi}) \approx \sum_{i=1}^{NN} \sum_{l=1}^{ND} \dot{E}_l^{\mathrm{e}i} \boldsymbol{N}_l^i(\boldsymbol{\xi}), \quad \boldsymbol{E}(\boldsymbol{\xi}) \approx \sum_{i=1}^{NN} \sum_{l=1}^{ND} E_l^{ei} \boldsymbol{N}_l^i(\boldsymbol{\xi}), \tag{15}$$

$$\ddot{\boldsymbol{B}}(\boldsymbol{\xi}) \approx \sum_{i=1}^{NN} \sum_{l=1}^{ND} \ddot{B}_l^{\mathrm{e}i} \boldsymbol{N}_l^i(\boldsymbol{\xi}), \qquad \boldsymbol{B}(\boldsymbol{\xi}) \approx \sum_{i=1}^{NN} \sum_{l=1}^{ND} B_l^{ei} \boldsymbol{N}_l^i(\boldsymbol{\xi}), \tag{16}$$

$$\dot{\Theta}(\boldsymbol{\xi}) \approx \sum_{i=1}^{NN} \dot{\Theta}^{ei} \boldsymbol{N}^i(\boldsymbol{\xi}), \quad \Theta(\boldsymbol{\xi}) \approx \sum_{i=1}^{NN} \Theta^{ei} \boldsymbol{N}^i(\boldsymbol{\xi}). \tag{17}$$

The vector $\boldsymbol{\xi}$ represents the natural coordinates and the superscript ^{ei} embodies the node values i of the element e. Moreover, the nodal quantities (15) and (17) are summarized in the vector $\mathbf{u}^{ei} = \left[\mathbf{E}^{ei}, \mathbf{B}^{ei}, \Theta^{ei}\right]$ and its time derivatives. The insertion of those approximations in equation (13), the integration over the element domain Ω^e via the GAUSS-LEGENDRE quadrature, the assembly over all elements and the application of the fundamental lemma of variational calculus leads to the linearized semidiscrete system of equations

$$\mathbf{M}\Delta\ddot{\mathbf{u}} + \mathbf{D}\Delta\dot{\mathbf{u}} + \mathbf{K}\Delta\mathbf{u} = \mathbf{r} - \mathbf{r}_{\mathrm{int}} \tag{18}$$

The matrices $\mathbf{M}, \mathbf{D}$ and $\mathbf{K}$ contain entries of the electric, magnetic and thermal field with respect to the second, first and zeroth time derivative. The outer flux vector is described by $\mathbf{r}$ and the inner flux vector by $\mathbf{r}_{\mathrm{int}}$. $\Delta\ddot{\mathbf{u}}, \Delta\dot{\mathbf{u}}$ and $\Delta\mathbf{u}$ are the increments of the variables and its time derivatives.

3.3 TEMPORAL DISCRETIZATION

For the numerical time integration of the linearized semidiscrete initial boundary value problem (18) the time interval of interest $t \in [t_0, T]$ is subdivided into NT constant or adaptively controlled time intervals $[t_n, t_{n+1}]$ with $n \in [0, NT]$ and the time step size $\Delta t = t_{n+1} - t_n$. Between two subsequent time intervals $[t_{n-1}, t_n]$ and $[t_n, t_{n+1}]$ the continuity conditions of the primary variable $\mathbf{u}$ and its time derivative $\dot{\mathbf{u}}$

$$[\![\mathbf{u}_n]\!] = \mathbf{u}_n^1 - \mathbf{u}_n^0 = 0, \qquad [\![\dot{\mathbf{u}}_n]\!] = \dot{\mathbf{u}}_n^1 - \dot{\mathbf{u}}_n^0 = 0, \tag{19}$$

are formulated as the difference of the right and left limiting values of the associated state variables at the time interval boundary, cf. [13]. The discontinuous formulations of GALERKIN time integration schemes satisfy these continuity conditions (19) in a weak sense, which means that nodal values of the primary variable $\mathbf{u}$ and its time derivative $\dot{\mathbf{u}}$ suffer from jumps across the boundaries. On the contrary the continuous GALERKIN methods fulfill the continuity in a strong fashion, cf. [15].

The transformation of the semidiscrete equilibrium equation (18) into the temporal weak form is accomplished by multiplication with an arbitrary vector valued weight function $\mathbf{w}(t)$ as well as its time derivative $\dot{\mathbf{w}}(t)$ and the integration over the time interval $[t_n, t_{n+1}]$, cf.[13]. The continuity condition (19) at the time element boundary is only weakly enforced by using the weight $\mathbf{w}^1 = \mathbf{w}(t_n)$ for the continuity of the primary variable $\mathbf{u}$ and the derivative of the weight $\dot{\mathbf{w}}^1 = \dot{\mathbf{w}}(t_n)$ for the derivative of the primary variable $\dot{\mathbf{u}}$. Finally, the weak formats of the equation of motion and the continuity conditions are added using the weight matrices $\mathbf{A}_u$ and $\mathbf{A}_v$.

$$\delta \mathbf{W} = \int_{t_n}^{t_{n+1}} \dot{\mathbf{w}} \cdot [\mathbf{M}\Delta\ddot{\mathbf{u}} + \mathbf{D}\Delta\dot{\mathbf{u}} + \mathbf{K}\Delta\mathbf{u} + \mathbf{r}_{\text{int}} - \mathbf{r}]\, dt \tag{20}$$

$$+ \qquad \dot{\mathbf{w}}_n^1 \cdot \mathbf{A}_{\text{v}}[\![\dot{\mathbf{u}}_n^k]\!] + \mathbf{w}_n^1 \cdot \mathbf{A}_{\text{u}}[\![\mathbf{u}_n^k]\!] + \mathbf{w}^1 \cdot \mathbf{A}_{\mathbf{u}}\Delta\mathbf{u}^1 + \dot{\mathbf{w}}^1 \cdot \mathbf{A}_{\dot{\mathbf{u}}}\Delta\dot{\mathbf{u}}^1 = 0 \tag{21}$$

These weight matrices are introduced to balance the summarized weak forms and to align their physical units, cf. [13, 16]. For the numerical solution of the weak form (20) approximations for state variables, test functions and their time derivatives are introduced in dependence of a natural time coordinate $\xi_t \in [-1,\ 1]$, cf. [16].

$$\ddot{\mathbf{u}}(\xi_t) \approx \sum_{j=1}^{p_t+1} N_{,tt}^j(\xi_t)\mathbf{u}^j, \qquad \dot{\mathbf{u}}(\xi_t) \approx \sum_{j=1}^{p_t+1} N_{,t}^j(\xi_t)\ \mathbf{u}^j, \qquad \mathbf{u}(\xi_t) \approx \sum_{j=1}^{p_t+1} N^j(\xi_t)\ \mathbf{u}^j \tag{22}$$

$$\dot{\mathbf{w}}(\xi_t) \approx \sum_{j=1}^{\bar{p}_t+1} \bar{N}_{,t}^j(\xi_t)\ \mathbf{w}^j, \qquad \mathbf{w}(\xi_t) \approx \sum_{j=1}^{\bar{p}_t+1} \bar{N}^j(\xi_t)\ \mathbf{w}^j \tag{23}$$

The approximations of the increments are carried out in the same way. Thus, one dimensional shape functions, GAUSS points and weights can be applied as in the standard spatial finite element method. A more detailed derivation for linear systems of equations of second order in time can be seen in [8] and nonlinear systems of equations of the first order in time are introduced in [16].

3.4 ERROR ESTIMATION

As a substantial ingredient of reliable time integration methods, local a-posteriori error measures are developed. For example, simultaneously performed time integrations of distinct accuracy based on the h-method can provide a local time integration error. These comparable solutions are calculated by using a smaller time step size $\Delta t/m$ with $m \in [2, 3, ...]$, cf. [15]. It is worth to mention that this error measure is on the one hand very reliable but on the other it require a very high numerical effort. Consequently, it is not very useful in practical applications.

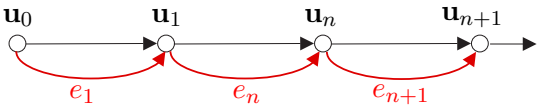

Figure 2: Illustration of the functionality of the residual error estimator

In order to formulate an efficient error estimate, the residual error estimate, originally proposed by Babuška & Rheinboldt [2] for the error estimation of the spatial finite element method, is adapted to the discontinuous and continuous Galerkin time integration schemes.

$$\mathbf{e}_{\mathrm{n}} = \int_{-1}^{1} \left[\mathbf{r}(\mathbf{u}(\xi_t)) - \mathbf{r}_{\mathrm{int}}(\ddot{\mathbf{u}}(\xi_t), \dot{\mathbf{u}}(\xi_t), \mathbf{u}(\xi_t))\right] \, |J_t| \, d\xi_t \tag{24}$$

The advantage of this error estimator is, that the residual error doest not require comparative calcultions, because the direct use of the calculated variables $\ddot{\mathbf{u}}, \dot{\mathbf{u}}$ and $\mathbf{u}$ in the nonlinear equation of motion yields the absolute error in the time interval, see **Figure 2**. In addition, it can also be decided whether the residual error of each field or of the whole problem is determined. Consequently, this error will be subject to further investigation. Scalar valued relative error measures are obtained by dividing the L_2-norm of the error vector $\mathbf{e}_{n+1}$ by a reference value e_{ref}. For example, the outer flux vector can be used as a reference.

$$\hat{\mathbf{e}}_{\mathrm{n}} = \int_{-1}^{1} \mathbf{r}(\xi_t) \, |J_t| \, d\xi t, \qquad\qquad e_{\mathrm{ref}} = \|\hat{\mathbf{e}}_n\| \tag{25}$$

4 SIMULATION OF INDUCTIVE HEATING PROCESS

4.1 NUMERICAL EXAMPLE OF A STEEL SHAFT

As a numerical example for the above deduced theory the inductive heating process of a 51CRV4 shaft, see **Figure 3**, with three rings as induction coil will be examined. Therefore, a sinusoidal current with an amplitude $I = 1231$ A and a frequency $f = 8100$ Hz will be applied to each of the induction rings. The initial temperature as well as the bulk temperature are $\Theta = 25°C$. Due to the changing current, the evolution of the electromagnetic and thermal field is calculated. Spatial discretization is realized

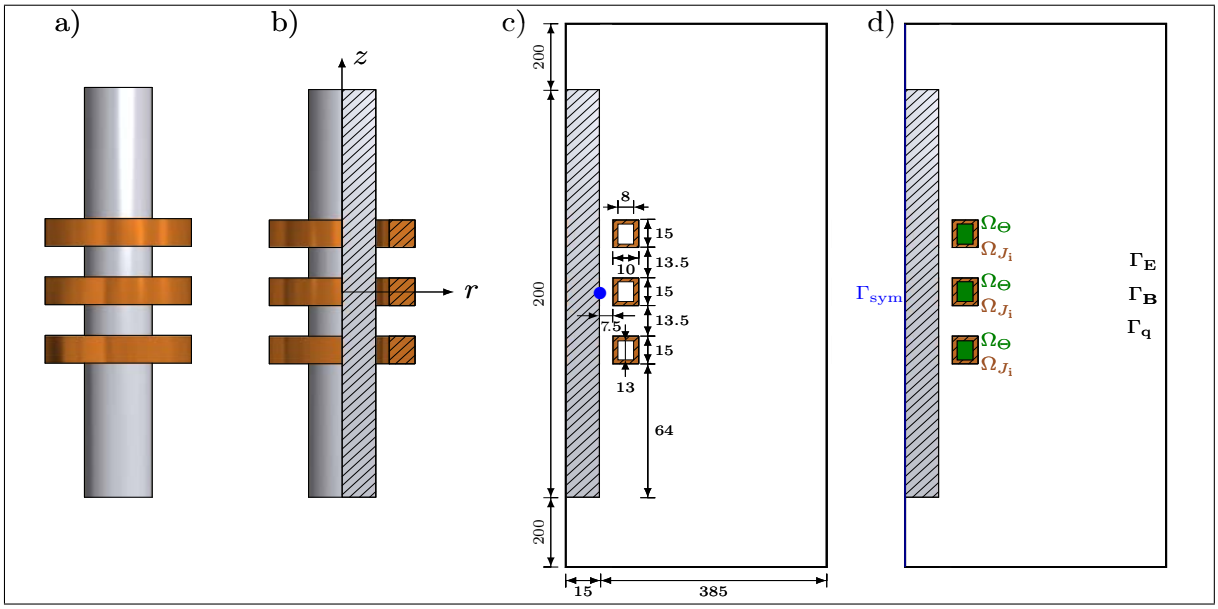

Figure 3: a) Axisymmetric depiction of the shaft, b) section of the shaft with coordinates (r, z), c) dimensions (in millimeters) of the model and d) DIRICHLET and NEUMANN boundary conditions

by quadrilateral LAGRANGE finite elements of polynomial degree $p = 2$. Furthermore, the present example is used to study the family of discontinuous p_t-GALERKIN time integration scheme with respect to robustness and order of accuracy. The necessary temperature dependent material parameters of the steel, air and copper are given in [10].

4.2 ELECTROMAGNETIC-THERMAL SOLUTION

Figure 4 shows an exemplary result of the electric, magnetic and thermal field. Therein it can be seen, that the electric and magnetic waves spread symmetrically starting at the induction coils and their influence decreases in all directions. While the magnetic field effects the whole steel shaft, the electric field penetrates the steel shaft only in the outer layer. Moreover, within certain time intervals almost the entire middle part of the steel shaft is effected by the electric field and consequently also by the source term distribution. In **Figure** 5 the evolution of the temperature distribution over the course of time is depicted. **Figure 6** demonstrates the solution (Point is indicated as a blue dot in **Figure 3** c)) of the field variables and its time derivatives. The lowest possible temporal polynomial degree is $p_t = 2$, which means that the primary variables are of quadratic nature, the first time derivative has a linear approximation and the second time derivative maintains a constant value throughout each time element. It can be seen, that the solution of the field variables and its time derivatives are improved with a decreasing time step size. The jumps between the time elements decreases also with a decrease in the time step size. **Figure 7** illustrates with an increasing polynomial degree an improvement of the quality of the solutions. A significant improvement can be seen in the second time derivative, because a linear approximation is now reached. Also a significant drop in the jumps between the polynomial degrees can be observed.

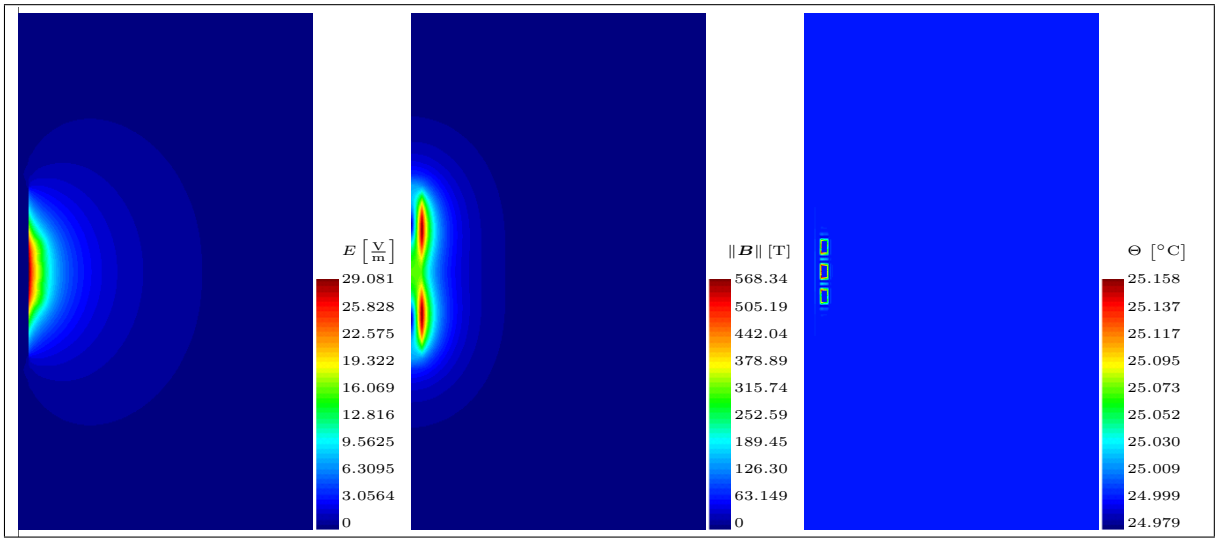

Figure 4: The electric field E, the magnetic field $\|\mathbf{B}\|$ and the temperature field Θ at time $t = 30\mu s$

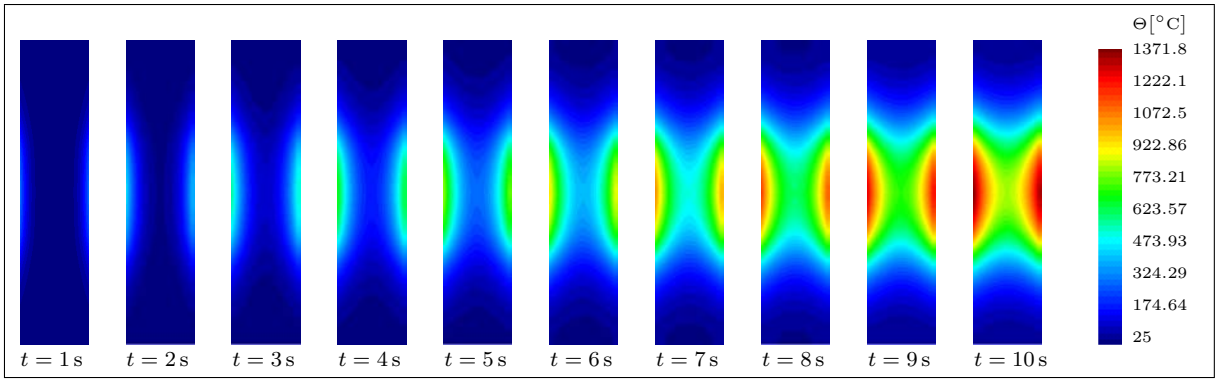

Figure 5: Chronological sequence of the temperature distribution in the steel shaft.

4.3 ERROR ANALYSIS

The improvement in the solutions with a decreasing time increment an/or the polynomial degree can also be confirmed with the help of the residual error estimator. **Figure 8** illustrates the residual error for the quadratic (left) and cubic (middle) approach. It can be seen, that the error becomes smaller with the time step size and it decreases for the same time increment with an increase of the temporal polynomial degree. The local order of convergence can be seen on the right hand side in **Figure 8**. The discontinuous GALERKIN methods demonstrate for different polynomial degrees a local order of $\mathcal{O}(\Delta t^3)$, $\mathcal{O}(\Delta t^4)$ and $\mathcal{O}(\Delta t^5)$. The residual error estimator of the discontinuous GALERKIN method has with the initial outer flux vector $\mathbf{r}(t = t_0)$ as the reference (25) measure accordingly a local order of convergence of $\mathcal{O}(\Delta t^{p_t+1})$. Thus, the residual error estimator provides a global order of convergence of $\mathcal{O}(\Delta t^{p_t})$.

5 CONCLUSION

In this paper the residual error for the inductive heating process with the GALERKIN method was shown. Therefore, the MAXWELL equations and the heat conduction equation were derived for the coupled electric, magnetic and thermal field. In the next step the p

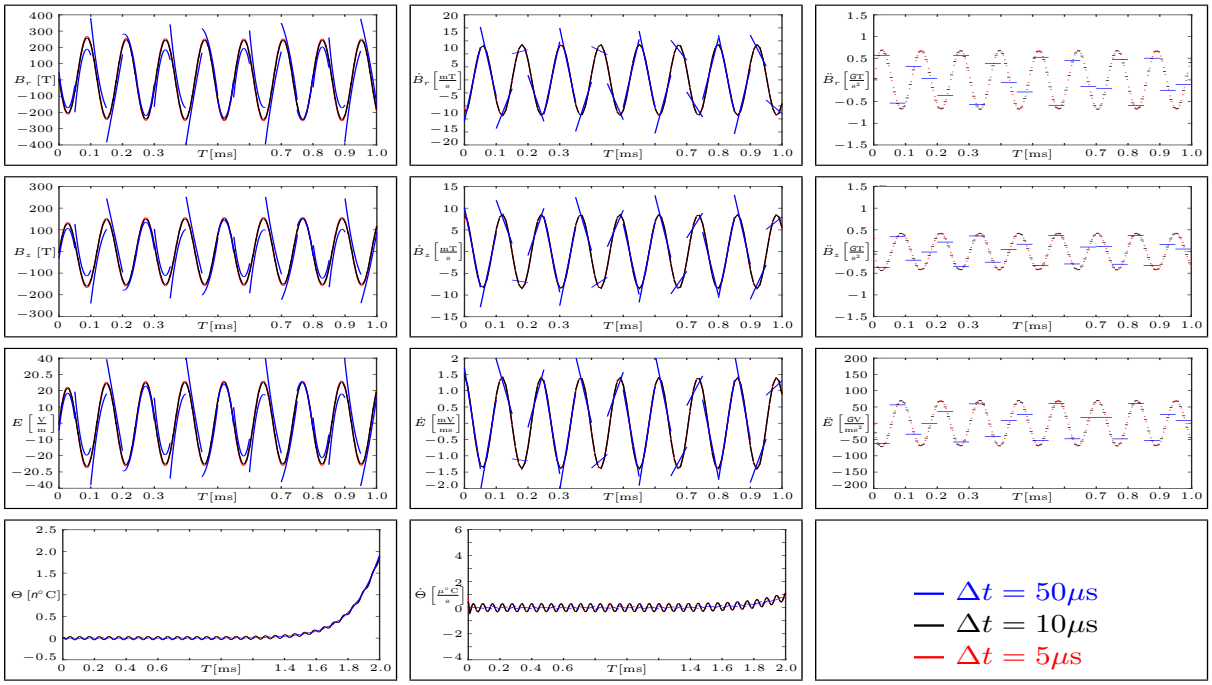

Figure 6: Time sequence of the field varialbes and their time derivatives using the discontinuous GALERKIN method dG(2)

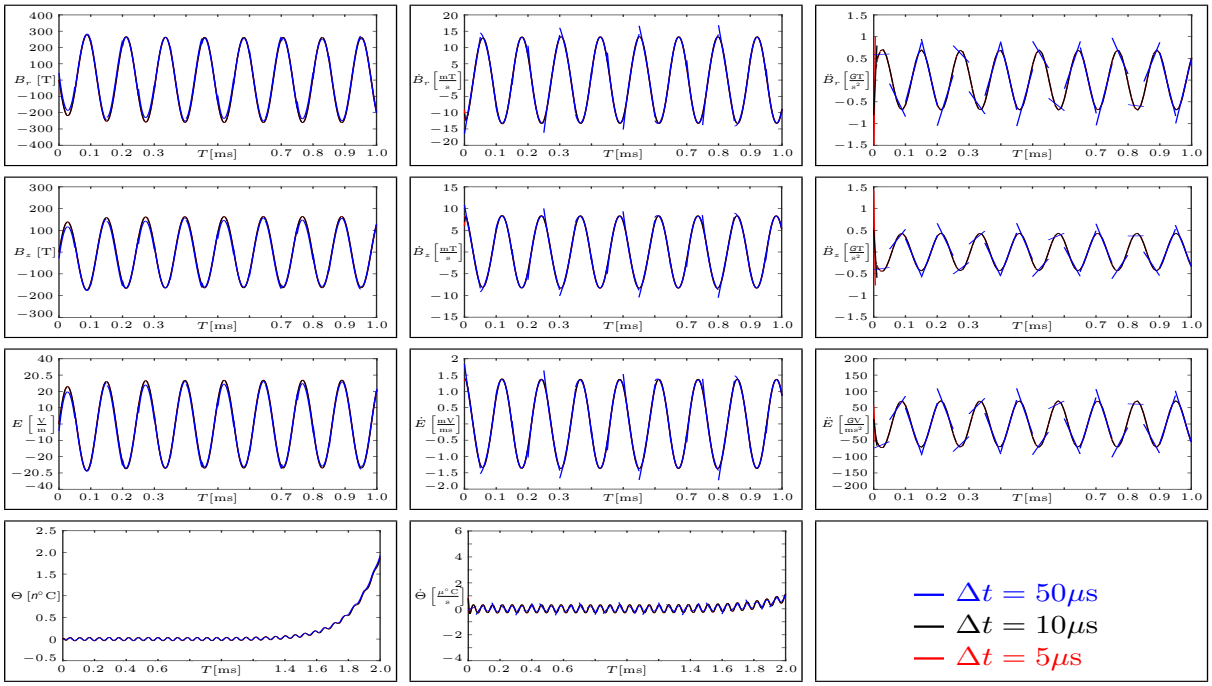

Figure 7: Time sequence of the field varialbes and their time derivatives using the discontinuous GALERKIN method dG(3)

finite element method was used for spatial discretization and discontinuous p_t-GALERKIN time integration schemes were presented within a generalized framework. Solutions of the inductive heating process for the electromagnetic and thermal field were demonstrated.

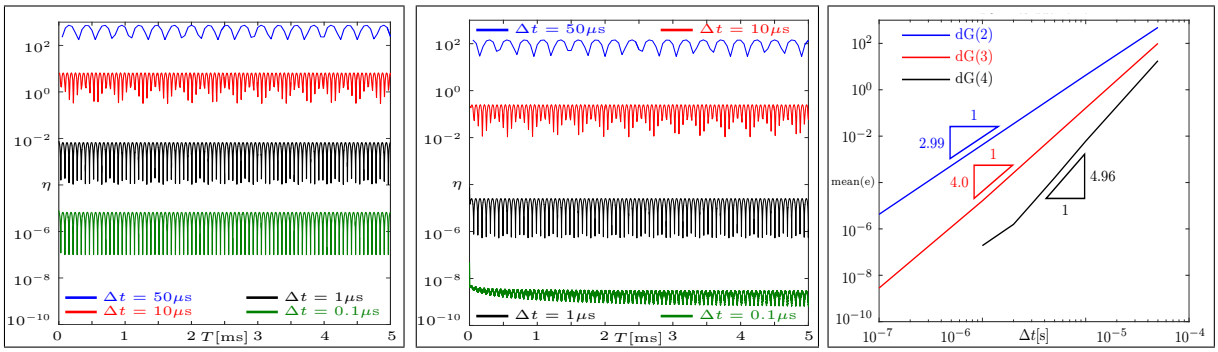

Figure 8: Residual error of dG(2) (left) and dG(3) (middle) of all fields added together and plotted over time for different time step sizes and local order of convergence for different polynomial degrees (right)

Additionally, numerical studies were carried out to show the dependency of the convergence rate on the polynomial degree p_t and the time step size Δt. These analyses have demonstrated that the applied GALERKIN time integration schemes lead to robust and higher order accurate numerical simulations of induction heating. Furthermore, the ability of the present BABUŠKA & RHEINBOLDT type error estimator to predict the time integration error and, consequently, the convergence rate of the investigated time integration methods was illustrated.

REFERENCES

[1] Assous, F., Ciarlet, P., Labrunie, S. and Sergé, J. Numerical solution to the time-dependent Maxwell equations in axisymmetric singular domains: The singular complement method. *Journal of Computational Physics.* (2003) **191**:147-176.

[2] Babuška, I. and Rheinboldt, C. A-posteriori error estimates for the finite element method. *International Journal for Numerical Methods in Engineering.* (1978) **12**:1597-1615.

[3] Birken, P., Gleim, T., Kuhl D. and Meister A. Fast Solvers for Unsteady Thermal Fluid Structure Interation. *International Journal for Numerical Methods in Fluids* (2015) **79**:16-29.

[4] Ciarlet, P. Jr. Augmented formulations for solving Maxwell equations. *Computer Methods in Applied Mechanics and Engineering.* (2005) **194**:559-586.

[5] Beck, R., Deuflhard, P., Hiptmair, R., Hoppe, R.H.W. and Wohlmuth, B. Adaptive multilevel methods for edge element discretizations of Maxwells equation, *Surveys of Mathematics for industry.* (1995).

[6] Demkowicz, L. *Computing with hp-adaptive finite elements: Volume 1: One and two dimensional elliptic and Maxwell problems.* (2007) Chapman & Hall/CRC Applied Mathematics and Nonlinear Science Series.

[7] Elsherbeni, A. and Demir, V. *The Finite Difference Time Domain for Electromagnetics: With Matlab Simulations.* (2008) SciTech Publishing Incorporated.

[8] Gleim, T. and Kuhl, D. Higher order accurate discontinuous and continuous p-Galerkin methods for linear elastodynamics. *Zeitschrift für angewandte Mathematik und Mechanik.* (2013) **93**:177-194.

[9] Gleim, T. *Simulation of Manufacturing Sequences of Functionally Graded Structures.* kassel university press, (2017).

[10] Gleim, T. and Kuhl, D. Electromagnetic Analysis Using Higher Order Numerical Schemes in Space and Time. *Archives of Computational Methods in Engineering* (2018) https://doi.org/10.1007/s11831-017-9249-9.

[11] Hoffman, J. *Adaptive Finite Element Methods for the Unsteady Maxwell's Equations.* Chalmers University of Technology (2000).

[12] Holzapfel, G. A. *Nonliner Solid Mechanics.* John Wiley & Sons, (2000).

[13] Hughes,T.J.R. and Hulbert,G.M. Space-time finite element methods for elastodynamics: Formulations and error estimates. *Computer Methods in Applied Mechanics and Engineering* (1988) **66**:339-363.

[14] Jamet, P. Galerkin-Type Approximations which are Discontinuous in Time for Parabolic Equations in a Variable Domain. *SIAM Journal on Numerical Analysis.* (1978) **15**:912-928.

[15] Kuhl, D. *Modellierung und Simulation von Mehrfeldproblemen der Strukturmechanik.* Shaker Verlag, (2004).

[16] Kuhl, D. and Meschke, G. Numerical analysis of dissolution processes in cementitious materials using discontinuous and continuous Galerkin time integration schemes. *International Journal for Numerical Methods in Engineering.* (2007) **69**:1775-1803

[17] Rudnev, V., Loveless, D., Cook, R. and Black, M. *Handbook of Induction Heating.* Marcel Dekker Inc, (2003).

[18] Schrder, B. and Kuhl, D. Small strain plasticity: classical versus multifield formulation. *Archive of Applied Mechanics* (2015) **85**, pp. 1127-1145.

[19] Stein, E. *Error-controlled Adaptive Finite Elements in Solid Mechanics.* John Wiley & Sons Ltd, (2003).

[20] Steinhoff, K., Weidig, U. and Saba, N. *Investigation of Plastic Forming Under the Influence of Locally and Temporally Variable Temperature and Stress States.* In: Functionally Graded Materials in Industrial Mass Production, Verlag Wissenschaftliche Scripten, (2009).

[21] Zienkiewicz, O.C and Taylor, R.L. *The Finite Element Method.* McGraw Hill, Vol. I., (1989).